

Improved Interpretation of Stark Broadening Data from Detached Divertor Plasmas

S. Lisgo, N. Brooks, E. Oks, M. Groth, A. W. Leonard et al.

Citation: *AIP Conf. Proc.* **874**, 253 (2006); doi: 10.1063/1.2402777

View online: <http://dx.doi.org/10.1063/1.2402777>

View Table of Contents: <http://proceedings.aip.org/dbt/dbt.jsp?KEY=APCPCS&Volume=874&Issue=1>

Published by the [American Institute of Physics](#).

Related Articles

Fast relaxation of the velocity distribution function of neutral and ionized species in high-power impulse magnetron sputtering

Appl. Phys. Lett. **99**, 131504 (2011)

Extracting 2D IR frequency-frequency correlation functions from two component systems

J. Chem. Phys. **135**, 074502 (2011)

Langevin–Bloch equations for a spin bath

J. Chem. Phys. **134**, 094114 (2011)

Time-dependent density functional theory of open quantum systems in the linear-response regime

J. Chem. Phys. **134**, 074116 (2011)

Anomalous strong exchange narrowing in excitonic systems

J. Chem. Phys. **134**, 034901 (2011)

Additional information on AIP Conf. Proc.

Journal Homepage: <http://proceedings.aip.org/>

Journal Information: http://proceedings.aip.org/about/about_the_proceedings

Top downloads: http://proceedings.aip.org/dbt/most_downloaded.jsp?KEY=APCPCS

Information for Authors: http://proceedings.aip.org/authors/information_for_authors

ADVERTISEMENT

**AIP Advances**

Submit Now

**Explore AIP's new
open-access journal**

- **Article-level metrics
now available**
- **Join the conversation!
Rate & comment on articles**

Improved Interpretation of Stark Broadening Data from Detached Divertor Plasmas

S. Lisgo^{1,2}, N. Brooks³, E. Oks⁴, M. Groth⁵, A.W. Leonard³, D. Volodko⁴,
and the DIII-D Team

¹University of Toronto Institute for Aerospace Studies, Toronto, M3H 5T6, Canada

²UKAEA Fusion Association, Culham Science Centre, Abingdon, Oxon OX14 3DB, UK

³General Atomics, San Diego, California 92186-5608, USA

⁴Physics Department, Auburn University, Auburn, AL 36849-5311, USA

⁵Lawrence Livermore National Laboratory, Livermore, California 94550, USA

Abstract. Stark broadening analysis of high- n Balmer series transitions ($n \rightarrow 2$, where $n = 6-10$) in deuterium is benchmarked against electron density measurements from a Thomson scattering system in the divertor region of the DIII-D tokamak. The time-averaged Thomson data show $n_e = (6.0 \pm 1.1) \times 10^{20} \text{ m}^{-3}$ in the low T_e region ($\sim 1 \text{ eV}$) of a detached divertor plasma. Analysis of the measured, Stark-broadened, Balmer-series line widths using the *conventional* theory gives $n_e = (4.5 \pm 0.9) \times 10^{20} \text{ m}^{-3}$. A more accurate analysis technique, referred to here as the *highly-advanced* theory (HAT) [E. Oks, *Stark Broadening of Hydrogen and Hydrogenlike Spectral Lines in Plasmas: The Physical Insight*, Alpha Science International, Oxford, UK, 2006], produces $n_e = (5.0 \pm 0.5) \times 10^{20} \text{ m}^{-3}$. In addition, a temperature of $(1.5 \pm 0.5) \text{ eV}$ is determined (the conventional theory does not allow deducing the temperature). Also the HAT reproduces the shape of the dependence of the measured width of the high- n Balmer lines on the principal quantum number n much better than the conventional theory. The improved diagnostic results favor the employment of the HAT when analyzing Stark broadening data from tokamak divertors.

Keywords: Stark broadening, tokamak, DIII-D, Thomson scattering

PACS: 39.30.+w, 52.55.Fa

INTRODUCTION

The lifetime of plasma facing components is a critical issue for next-generation fusion devices, including the proposed International Thermonuclear Experimental Reactor, ITER [1]. The physics solution for the steady-state heat flux to the divertor target plates, where the plasma-material surface interactions are concentrated, involves operating with a detached plasma, which is characterized by low plasma temperatures and a reduced ion flux to the target [2]. Unfortunately, a quantitative understanding of detachment has proved elusive, hampering efforts to accurately predict detached divertor performance in next-step machines.

The Alcator C-Mod tokamak utilizes a high magnetic field that allows operation at higher core densities than other devices; these high core densities naturally give rise, with the limited auxiliary heating power available on C-Mod, to cold, detached plasmas in the divertor region. Detailed

CP874, *Spectral Line Shapes: 18th International Conference*,

edited by E. Oks and M. Pindzola

© 2006 American Institute of Physics 978-0-7354-0370-3/06/\$23.00

spectroscopic studies of detachment were carried out in an effort to characterize the associated plasma conditions [3-5], with electron temperatures of $T_e \approx 0.5$ eV in the divertor volume obtained by fitting the distribution of high- n Balmer emissions to the Saha equation (where “ n ” is the principal quantum number of the upper level), and electron densities of $n_e = (0.5\text{--}2.0) \pm 0.3 \times 10^{21} \text{ m}^{-3}$ deduced from Stark broadening of the same lines using conventional theory [6,7]. The full spectroscopic and Langmuir probe data sets were compared with output from the OSM-EIRENE “plasma reconstruction” code, but agreement was only marginally within experimental uncertainties [8]. Accurate measurement and simulation are critical for detached plasma analysis because volume recombination processes can be significant below ~ 1 eV and are highly nonlinear in both n_e and T_e [9].

In order to evaluate the accuracy of the Stark broadening analysis methods, the study has been repeated on the DIII-D tokamak [10], where the divertor is fitted with a Thomson scattering system [11] that can provide an independent measurement of n_e .

EXPERIMENTAL SETUP

DIII-D is a medium size diverted tokamak with major radius $R = 1.66$ m and minor radius $a = 0.67$ m. The discharge being investigated has a lower single null in the poloidal magnetic field, line averaged electron density $\bar{n}_e = 8.1 \times 10^{19} \text{ m}^{-3}$ during the flat-top, an axial toroidal field of $B_T = 2$ Tesla, plasma current of $I_p = 1.1$ MA, and 6.6 MW of neutral beam heating, with the $B \times VB$ drift toward the lower divertor. Time traces of the principal plasma parameters are shown in Fig. 1. Enhanced confinement, or H-mode, is indicated by the regular D_α fluctuations that are characteristic of H-mode related Edge Localized Modes, or ELMs [12]. These ELMs are associated with periodic bursts of particles and energy out of the confined plasma, which are then transported to the walls of the vacuum vessel. The average time between ELMs, τ_{ELM} , for this discharge is ~ 5 ms.

A schematic cross-section of the lower divertor is presented in Fig. 2, along with the diagnostic lines-of-sight that are of interest here.

The line shapes of the high- n Balmer series lines ($n \rightarrow 2$, with n ranging from 6 to 10) are measured in the wavelength interval $397 < \lambda < 410$ nm along a vertical path through the divertor at $R = 1.49$ m. The Czerny-Turner spectrometer has an instrumental broadening of ~ 0.2 nm and a dispersion of 0.0226 nm/pixel. The divertor plasma density is high enough in this discharge, and the temperature low enough, that the high- n Balmer lines exhibit Stark broadening that is significantly greater than the instrumental broadening. Unfortunately, the spectrometer integration time is 10 ms, or approximately two ELM periods, and so the measured FWHMs of these lines are always ELM-averaged quantities, complicating the analysis; see Section 3.

The divertor Thomson scattering (DTS) system views the electron-scattered light from a Nd:YAG laser at eight points along its vertical path, measuring n_e and T_e (for $T_e > \sim 1$ eV). Each laser pulse lasts only 10 ns, a duration much shorter than τ_{ELM} ; the laser pulse repetition rate is 50 Hz. The laser is at the same radial location as the high-resolution spectrometer view, but displaced toroidally, allowing a direct comparison of $n_{e,\text{Stark}}$ and $n_{e,\text{DTS}}$ at identical points in the poloidal plane.

The tomographic inversion of a tangentially viewing 2D CCD camera image gives the poloidal distribution of D_γ ($5 \rightarrow 2$) in the divertor [13,14]; see Fig. 3, where the inversion was performed for

a 1 ms integration over the ELM peak. Assuming D_γ to be representative of the higher- n Balmer lines, the emission along the spectrometer line-of-sight is clearly localized to the private-flux region (PFR) below the x-point. As a result, only channels 0–3 of the DTS system need to be considered in the present analysis. These high levels of D_γ emission indicate that the divertor is partially detached on both the inner and outer target plates.

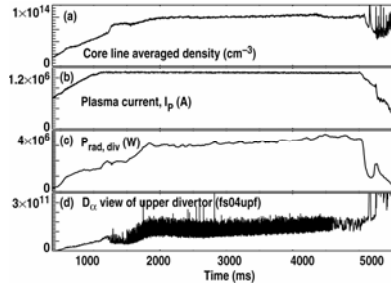


FIGURE 1. Relevant time traces for discharge 123410. (a) Average plasma density in the confined plasma (core), (b) plasma current, (c) radiated power in the divertor region, (d) fast D_α trace (20 kHz sampling) in the upper divertor (a lower divertor view was not available). The high-frequency D_α fluctuations indicate rapid ELMs.

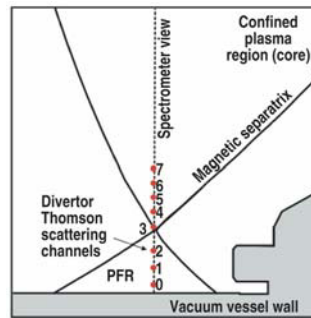


FIGURE 2. Schematic of a poloidal cross-section of the DIII-D lower divertor region. The high-resolution spectrometer view (dashed line) and divertor Thomson channels (dots, marked 0 to 7) are shown. The “separatrix” is the last closed magnetic flux surface, and marks the interface between the confined plasma and the boundary plasma that interacts with the walls of the containment vessel. The private flux region (PFR) is below the x-point and between the legs of the separatrix.

ANALYSIS OF DIVERTOR THOMSON DATA

As stated in the introduction, the objective is to compare estimates of n_e from Stark broadening analysis with n_e data from DTS, in an effort to evaluate the accuracy of competing Stark broadening models. Unfortunately, the divertor plasma fluctuations related to ELMs are substantial, as seen in Fig. 1d, which means that the measured Stark broadened density is a function of the density variation over the ELM. Therefore, a comparison with $n_{e,DTS}$ requires the calculation of a weighted average ($\tau_{DTS} \ll \tau_{ELM}$) over the ELM:

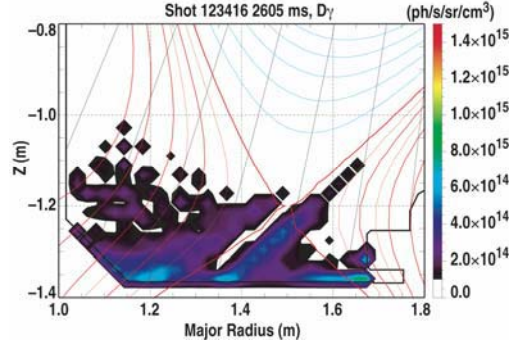


FIGURE 3. Tomographic inversion of 2D CCD tangentially viewing camera image of the divertor, in D_γ light. The emission is concentrated in the PFR, so that only this region needs to be considered in the DTS analysis. Reproduced from [15], courtesy of M. Groth.

$$\langle n_{e,div} \rangle = \int_{Z_0}^{Z_x^{t_{ELM}}} \int_0^{t_{ELM}} \varepsilon(Z, t) n_{e,div} dt dZ, \quad (1)$$

where Z is the vertical coordinate along the line-of-sight, t is time, and ε is the normalized emissivity of the high- n Balmer line that is used as the weight function. The spatial variation of the divertor plasma along the spectrometer view, as indicated by the D_γ inversion in Fig. 3, is (coarsely) resolved by the four DTS channels between the x-point and the divertor floor. The DIII-D discharge being investigated was successfully repeated 22 times, giving excellent samples of the temporal variations of n_e and T_e over the ELM cycle.

The DTS data for channels 0 to 3 are plotted in Fig. 4 as a function of the time elapsed between the laser pulse and the start of the previous ELM, τ_{ELM} , which is determined from a library of ELM profile analysis tools [16]. The DTS measurements are filtered so that data were plotted only for typical ELMs, i.e. where the D_α peak is less than 1 ms after the start of the ELM and the time to the start of the next ELM is 4.5–6 ms.

The polynomial fits to the DTS data in Fig. 4 are interpolated along Z in order to produce $n_e(Z, t)$ and $T_e(Z, t)$ profiles along the spectrometer line-of-sight, with linear interpolation results shown in Fig. 5. The $\varepsilon(n_e(Z, t), T_e(Z, t))$ values in Equation (1) are then set to the emissivity for a given high- n Balmer transition using the ADAS database [17]; see Fig. 5c. Given the detached divertor plasma conditions in these discharges, it is assumed that the high- n emissions are dominated by volume recombination processes and that $n_{D^+} = n_e$ locally.

Equation 1 is not the best method of calculating $\langle n_{e,div} \rangle$. Ideally, a Stark broadening model should be used to predict the line shape at each point along the spectrometer view, with the resultant superposition of line shapes compared to the measured profile (assuming instrumental and Zeeman broadening are properly taken into account). This exercise is relegated to future work.

The above exercise gives $\langle n_{e,div} \rangle = 6.0 \pm 0.5 \times 10^{20} \text{ m}^{-3}$ when only considering uncertainties related to the interpolation process. If the stated uncertainties in the individual DTS data measurements are also included, then the absolute error increases to $\langle n_{e,div} \rangle = 6.0 \pm 1.1 \times 10^{20} \text{ m}^{-3}$. The average density depends weakly on the particular high- n line that is used as the weight function.

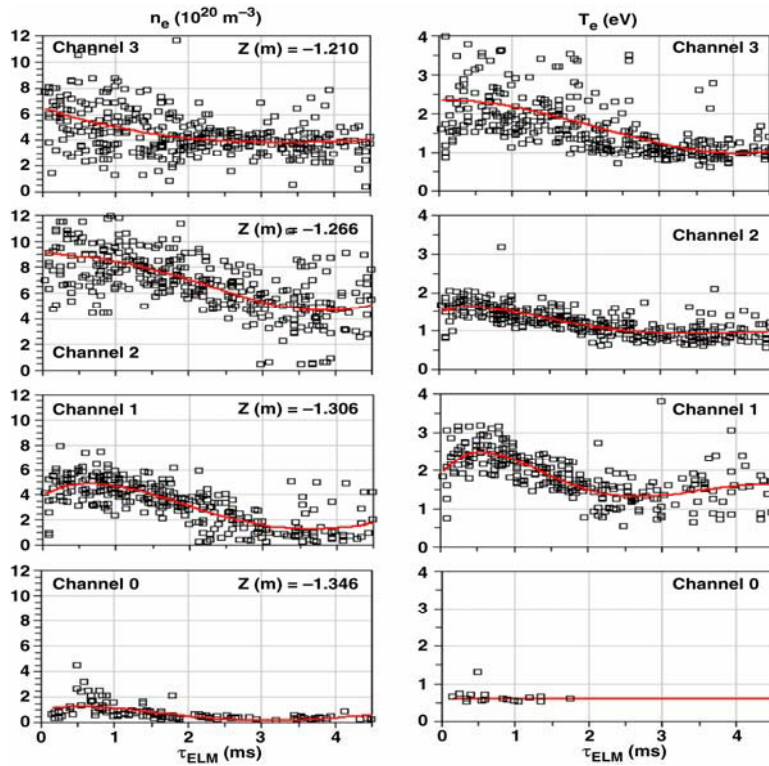


FIGURE 4. DTS n_e (left column) and T_e data plotted as a function of time since the start of the most recent ELM, relative to the associated laser pulse. The lines are polynomial fits to the data. The energy and particles expelled from the core during the ELM are apparent, although much of the energy has been dissipated by the dense plasma in the detached divertor. The low n_e indicated for channel 0 give spurious T_e data.

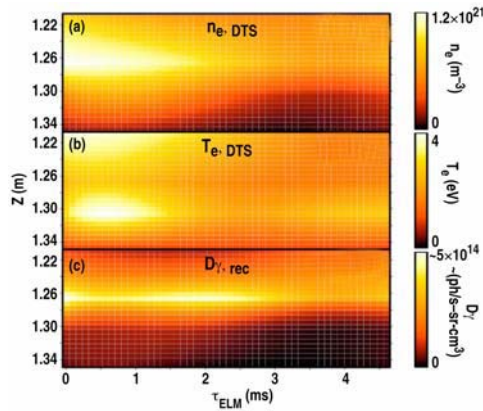


FIGURE 5. Divertor Thomson scattering data interpolated temporally over an ELM cycle and spatially between the lower divertor floor and x-point. The Balmer emission proves the weight function when averaging $n_{e,DTS}$ along the spectrometer line-of-sight. The D_γ signal from volume recombination is shown here, and there is little variation in the distribution for the higher- n lines.

MODELING OF STARK BROADENING OF HIGHLY-EXCITED BALMER LINES

Figure 6 shows the shapes of the measured deuterium Balmer lines $n \rightarrow 2$, with $n = 6-10$. Acceptable signal-to-noise was obtained by integrating over the period during which the x-point was held stationary and plasma conditions were constant.

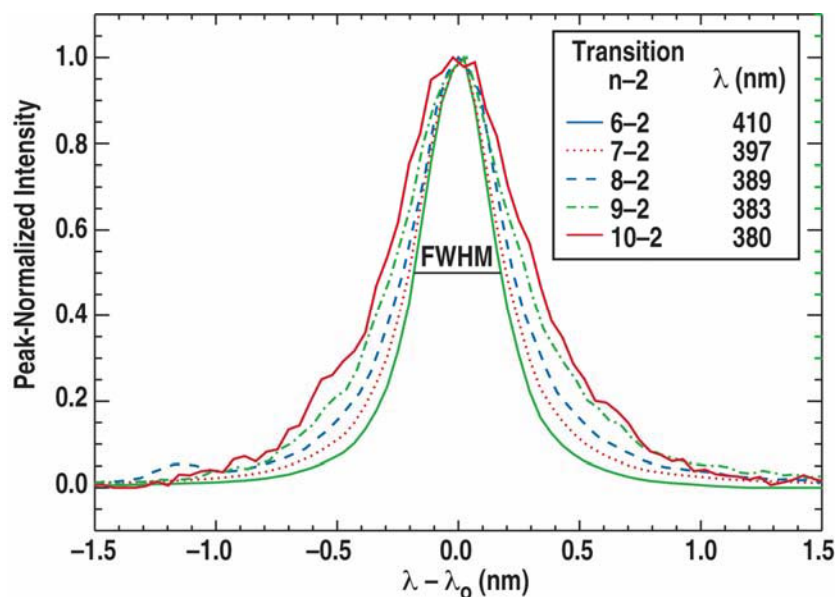


FIGURE 6. Profiles of high- n deuterium Balmer lines. The signals were integrated over the portion of the discharge during which conditions were held constant.

The experimental FWHM values from Fig. 6 are plotted versus n in Fig. 7. Also shown are fits from the “conventional” [7] and “highly-advanced” [18,19] Stark broadening theories.

The highly-advanced theory (HAT) [18,19] is based primarily on a generalization of the formalism of dressed atomic states (DAS) in plasmas. DAS is the formalism initially designed to describe the interaction of a monochromatic (or quasi-monochromatic) field – e.g., laser or maser radiation – with gases. Later it was applied for the interaction of a laser or maser radiation with plasmas [20]. The generalization of DAS consists in using atomic states dressed by a broad-band field of plasma electrons and ions [18,19] (rather than by a monochromatic field).

The employment of the generalized DAS by the HAT [18,19] enables an analytic description of the coupling between electron and ion microfields mediated by the radiating atom. This indirect coupling increases nonlinearly with the increase of the principal quantum number n and with the decrease of the temperature. Therefore it becomes important for high- n lines even at moderate electron densities.

Accurate analytical results for the ion-dynamical broadening are the second outcome of employing the generalized DAS in the HAT. The ion-dynamical broadening is obtained in a non-binary description of the ion microfield and without using the impact approximation. For the edge plasmas of tokamaks, the ion-dynamical corrections could be relatively significant for Balmer

lines originating from levels with $n < 8$ at the electron densities $n_e \sim 10^{20} \text{ m}^{-3}$ or for Balmer lines originating from levels with $n < 6$ at the electron densities $n_e \sim 10^{21} \text{ m}^{-3}$.

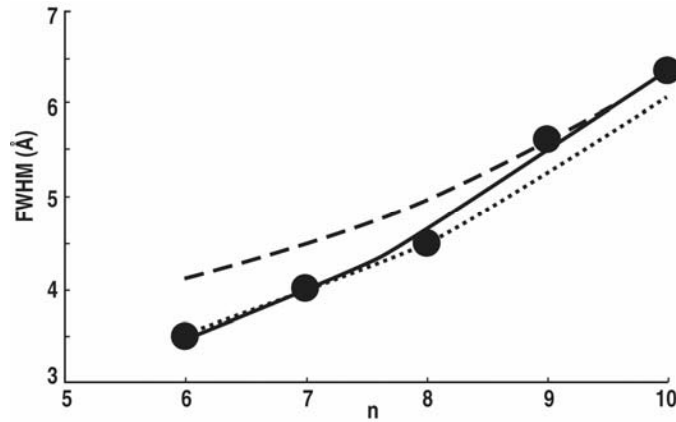


FIGURE 7. FWHM versus the principal quantum number, n , of deuterium high- n Balmer lines, as measured in the DIII-D divertor. Fits for Stark broadening theories are shown: highly-advanced theory with $n_e = 5.0 \times 10^{20} \text{ m}^{-3}$ and $T = 1.5 \text{ eV}$ (solid line), and conventional theory with $n_e = 3.9 \times 10^{20} \text{ m}^{-3}$ (dashed line) and $n_e = 5.1 \times 10^{20} \text{ m}^{-3}$ (dotted line).

For the above reasons the application of the HAT to the analysis of experimental high- n lines enhances the accuracy of the density determination and, additionally, yields the *temperature*, which the conventional theory doesn't provide at all.

From Fig. 7 it is seen that the HAT more accurately reproduces the shape of the experimental FWHM dependence than the conventional theory. The shape of the FWHM dependency in the HAT is generally more complicated than that in the conventional theory because of the competition of the two additional effects included in the HAT, but neglected in the conventional theory: indirect coupling and ion-dynamical broadening. Broadening due to the indirect coupling increases with n , while that due to the ion-dynamical broadening decreases with n .

Plasma parameters were obtained from the best fit to the shapes of the experimental Balmer lines presented in Fig. 6. The best fit for the conventional theory yields $n_{e,Stark} = (4.5 \pm 0.9) \times 10^{20} \text{ m}^{-3}$ and no information on the temperature. The most probable values of the densities, deduced from individual line profiles fitted by the conventional theory, vary by about 13%. The best fit for the HAT yields $n_{e,Stark} = (5.0 \pm 0.5) \times 10^{20} \text{ m}^{-3}$ and the temperature $T = 1.5 \pm 0.5 \text{ eV}$. The most probable values of the densities, deduced from individual line profiles fitted by the HAT, vary only by about 5%.

The plasma parameters deduced from the Stark broadening of the experimental high- n Balmer lines can be now compared with $\langle n_{e,div} \rangle = (6.0 \pm 1.1) \times 10^{20} \text{ m}^{-3}$ and $T_e = 1-2 \text{ eV}$ determined from the experimental DTS ELM data. It is seen that the latter agrees with the temperature deduced via the HAT (while the conventional theory was unable to deduce the temperature from the high- n lines) and also agrees with the electron density deduced via the HAT slightly better than with the electron density inferred via the conventional theory. Last but not least, the HAT reproduces the

shape of the dependence of the measured width of the high- n Balmer lines on the principal quantum number n much better than the conventional theory*/.

In the experimental profiles of the $9 \rightarrow 2$ and $10 \rightarrow 2$ lines (D_9 and D_{10}) one can discern slight “shoulders” – especially in the D_{10} profile. On the one hand, this could be a result of a spatial non-uniformity of the plasma along the line of sight, with the shoulders being emitted from a higher density region and the bulk of the line from a lower density region. On the other hand, for our experimental conditions, Balmer lines D_n with $n > 8$ could have some shoulders, though less pronounced than in our experimental profiles, even if the plasma were spatially uniform. In the discussion below a physical explanation is offered for slight shoulders in the case of a spatially uniform plasma.

The positions of Stark components of hydrogen/deuterium lines are controlled by (proportional to) the following combination of quantum numbers

$$X_{nn'} = nq - n'q', \quad (2)$$

where n and n' are the principal quantum numbers of the upper and lower energy levels, respectively; $q = n_1 - n_2$ and $q' = n'_1 - n'_2$ are the electric quantum numbers of the upper and lower Stark sublevels, respectively; n_1, n_2, n'_1, n'_2 are the standard parabolic quantum numbers defined in textbooks on quantum mechanics (see, e.g. [23], sect. 37). For the most intense Stark component of a given high- n line, in accordance to Ref. 20, page 121, one has $X_{nn}^{(1)} = n$ for the lines containing no central (“unshifted”) components ($n + n'$ is even) or $X_{nn}^{(1)} = 2n$ for all other high- n lines. Specifically, for the Balmer lines ($n' = 2$) corresponding to $n > 4$, one has:

$$X_{n2}^{(1)} = n \text{ (for even } n); \quad X_{n2}^{(1)} = 2n \text{ (for odd } n). \quad (3)$$

For the second most intense Stark component of the Balmer lines of $n > 4$, one has:

$$X_{n2}^{(2)} = n(n-1) - 2. \quad (4)$$

The ratio $X_{n2}^{(2)}/X_{n2}^{(1)}$ increases with n :

$$X_{n2}^{(2)}/X_{n2}^{(1)} = (n-1-2/n) \text{ (for even } n); \quad X_{n2}^{(2)}/X_{n2}^{(1)} = (n-1-2/n)/2 \text{ (for odd } n). \quad (5)$$

This means that as n increases, the second most intense Stark component moves farther out into the wings relative to the position of the most intense Stark component.

Now let us look at the ratio $I_{n2}^{(2)}/I_{n2}^{(1)}$ of the intensity $I_{n2}^{(2)}$ of the second most intense Stark component to the intensity $I_{n2}^{(1)}$ of the most intense Stark component. For $n > 4$, both within the sequence of odd n and within the sequence of even n , as n increases, this ratio $I_{n2}^{(2)}/I_{n2}^{(1)}$ first decreases, then reaches a minimum, and then increases. The ratio $I_{n2}^{(2)}/I_{n2}^{(1)}$ reached its minimum at $n = 7$ for odd n or at $n = 8$ for even n .

The increase of the ratio $I_{n2}^{(2)}/I_{n2}^{(1)}$ starting from $n = 9$ combined with the fact that the second most intense Stark component moves further to the wings relative to the position of the most intense Stark component as n increases is the underlying physical reason for possible shoulders in the Balmer lines of $n > 8$. However, these shoulders will show up only if the electron density is sufficiently low.

Indeed, the above reasons relate to quasistatically-broadened profiles of Balmer lines. The dynamical broadening (by most of the electrons and some of the ions) tends to smooth out any structure resulting from the quasistatic broadening, since the former scales essentially linearly with the electron density n_e , whereas the latter scales as $n_e^{2/3}$. Therefore, at sufficiently large electron densities, the dynamical broadening will smooth out any structure in quasistatic profiles, including the possible shoulders.

The fact that Stark profiles can have structures, such as peaks, dips and/or a second maximum/shoulder (in each wing of the line), is not new. The structures can be found both within the purely quasistatic calculations of 1959 [21] and within the calculations by the conventional theory of 1970 [6]. The latter fact had not been explicitly claimed in [6], but in paper [5] of 1995 - while discussing the calculations from [6]. It should be emphasized that the calculations performed in [5] by the conventional theory were conducted in a more approximate way than the calculations from [6]. Indeed, instead of profiles containing structures, yielded within the conventional theory by rigorous calculations in [6], the authors of [5] substituted such profiles by Lorentzians of the same halfwidth – as noted in [5]. Obviously, the Lorentzians do not have any structures. Therefore, the calculations from [5] could not reveal any structures at all.

Let us now discuss later calculations performed by various authors for modeling experimental profiles of high- n Balmer lines observed from divertors of other tokamaks. In papers [3] of 1998 and [4] of 1999, from fitting experimental profiles of high- n Balmer lines observed from the divertor of Alcator C-Mod, the authors deduced the electron density $n_e = (1.2 - 1.8) \times 10^{21} \text{ m}^{-3}$. The modeling of the profiles was done employing the approximate version of the conventional theory, in the same way as in [5]. Of course, such modeling cannot produce shoulders in the line profiles, as explained above. Besides, the higher electron density in the divertor of Alcator C-Mod divertor compared with DIII-D caused a significant overlap between the wings of adjacent high- n Balmer lines, making the profile fitting to individual high- n lines like D_9 and D_{10} more problematic than in the case of DIII-D. As for the experimental profiles, they did not show any shoulders. Most probably this was due to the fact that the electron density in the experiments [3, 4] was about three times higher than in the DIII-D experiment, so that the dynamical broadening would have smoothed out any possible shoulders.

In paper [22] of 2002, from fitting experimental profiles of high- n Balmer lines observed from the divertor of JET, the authors deduced the electron density $n_e = 8 \times 10^{19} \text{ m}^{-3}$. The modeling of the profiles was done employing the frequency fluctuation model (FFM). The FFM is much more advanced than the conventional theory. In this simulation model, closely lying Stark components of a spectral line are artificially bunched together and considered as one “radiative channel”. So, the spectral line is represented by these

radiative channels, the number of which is much smaller than the number of the Stark components, what simplifies the computations. The ion dynamics is then taken into account approximately by a mixing of the radiative channels via some stochastic Markovian process. Though only approximate in its description of ion dynamics and the structure of the Stark components and lacking entirely the coupling of electron and ion microfields contained in HAT, the FFM is usually much more accurate than the conventional theory. The profiles calculated by the FFM in [22] did not seem to show shoulders, perhaps due to the approximate treatment of the structure of the Stark components.

Coming back to the shoulders observed in the lines D_9 and D_{10} in our experiment: they could result either from a spatial non-uniformity of the plasma along the line of sight or - in the case of a quasi-uniform plasma - from the specific properties of the Balmer lines of $n > 8$ outlined above. This problem requires a further study.

DISCUSSION AND CONCLUSIONS

High resolution measurements of Stark broadened, high- n Balmer series lines were made for a rapidly ELMing plasma discharge. The ELM-averaged values of n_e deduced from Stark broadening analysis of the Balmer line profiles by the conventional theory and by the highly-advanced theory were compared with a column-averaged n_e derived from divertor Thomson scattering data. The n_e inferred via the highly-advanced theory is in better agreement with the DTS value than that inferred via the conventional theory. The temperature deduced from the highly-advanced theory gives good agreement with the DTS analysis, whereas the conventional theory of Stark broadening provides no information about temperature. Finally, the highly-advanced theory gave a significantly better match to the distribution of FWHM with n . Overall, the highly-advanced theory provided the best representation of the experimental data.

REFERENCES

1. ITER Expert Groups, *Nuclear Fusion* **39** (12), 2137-2627 (1999).
2. P. C. Stangeby, *Nuclear Fusion* **33** (11), 2503-2504 (1993).
3. J. L. Terry, B. Lipschultz, et al., *Physics of Plasmas* **5** (5), 1579 (1998).
4. B. Lipschultz, J. L. Terry, et al., *Physics of Plasmas* **6** (5), 1907 (1999).
5. B. L. Welch, H. R. Griem, et al., *Physics of Plasmas* **2** (11), 4246-4251 (1995).
6. R. Bengtson, J. D. Tannich and P. Kepple, *Physical Review A* **1**, 532 (1970).
7. H. R. Griem, *Spectral Line Broadening by Plasmas*, Academic Press, New York, 1974.
8. S. Lisgo, et al., *J. Nuclear Materials* **337** (1-3), 139-145 (2005).
9. S. Lisgo, "Interpretive Modeling of the Alcator C-Mod Divertor," Ph.D. Thesis, University of Toronto, 2003. <http://starfire.utias.utoronto.ca/divimp/publications/>
10. J. L. Luxon, T. C. Simonen, R. D. Stambaugh, *Fusion Science and Technology* **48** (2), 807-827 (2005).
11. S. L. Allen, D. N. Hill, T. N. Carlstrom, et al., *J. Nuclear Materials* **241**, 595-601 (1997).
12. W. Fundamenski, R. A. Pitts, et al., *Nuclear Fusion* **45** (8), 950-975 (2005).
13. M. Fenstermacher, W. H. Meyer, et al., *Review Scientific Instruments* **68** (1), 974-977 (1997).
14. M. Groth, M. E. Fenstermacher, et al., *J. Nuclear Materials* **313**, 1071-1075 (2003).
15. M. Groth, *DIII-D Science Meeting talk*, March 2006. groth@fusion.gat.com
16. G. D. Porter, T. A. Casper, J. M. Moller, *Physics of Plasmas* **8** (12), 5140-5150 (2001).
17. H. P. Summers, et al., *Plasma Physics and Controlled Fusion* **44**, B323-B338 (2002).
18. E. Oks, *Stark Broadening of Hydrogen and Hydrogenlike Spectral Lines in Plasmas: The Physical Insight*, Alpha Science International, Oxford, UK, 2006.
19. E. Oks, "Stark Widths of Hydrogen Lines in Plasmas: a Highly-Advanced Non-Simulative Semiclassical Theory and Tables," in *this Volume*.
20. E. Oks, *Plasma Spectroscopy: The Influence of Microwave and Laser Fields*, Springer, Berlin, 1005.
21. A.B. Underhill and J.M. Waddell, *National Bureau of Standards Circular No. 603*, Washington DC, 1959.
22. M. Koubiti, H. Capes, L. Godbert-Mouret, Y. Marandet, A. Meigs, S. Loch, R. Stamm, and H. Summers, "Diagnostics of Detached Plasmas Using High- n Lines and Continuum Spectral of D and He", in *Spectral Line Shapes v. 12*, edit. C.A. Back, AIP Conf. Proc. 645, AIP, New York, 2002, p. 67.
23. L. D. Landau and E. M. Lifshitz, *Quantum Mechanics*, Pergamon, Oxford, 1965.